Weak semileptonic decay distributions for new particles*

V. Barger
Physics Department, University of Wisconsin, Madison, Wisconsin 53706

R. J. N. Phillips
Rutherford Laboratory, Chilton, Oxon, England
(Received 23 February 1976)

We develop a general formalism for describing the $e\nu$ and $\mu\nu$ semileptonic decays of arbitrary unpolarized particles, and apply it in a discussion of the dilepton events produced in neutrino experiments. The formalism holds for mesons, baryons, or heavy leptons, with arbitrary spin and quantum numbers, decaying into exclusive or inclusive channels. Results are obtained for single-particle decay distributions. Specific examples of experimental interest are evaluated explicitly; in particular, for the decay $Y \to Ke\nu$, we calculate the Ke invariant-mass distribution and all single-particle momentum distributions transverse to either a plane or a line. To obtain the distributions of secondary leptons from the decaying Y particles in neutrino processes, we adopt the current-fragmentation quark-parton model for Y-meson production. Distribution broadening from Y transverse momentum is calculated. Estimates of the Y-particle mass are obtained from experimental transverse-momentum distributions of the slow muon in neutrino dimuon events. The true dimuon rate is estimated to be 2–3 times larger than the observed rate, because of the experimental acceptance cutoff at low muon energy.

I. INTRODUCTION

The origin of $\mu^-\mu^+$ and $\mu^-e^+K_S^0$ dilepton events in neutrino experiments[1-4] is almost certainly the production and subsequent weak decay of hadrons with new quantum numbers, referred to as Y particles.[1] In order to analyze these processes and extract quantitative information about the masses, decay properties, and production mechanisms of Y, it is first necessary to have a sufficiently general approach to the Y decay process.

In this paper we develop a general formalism for the decay of an arbitrary unpolarized particle (meson, baryon, or heavy lepton) into exclusive or inclusive semileptonic $e\nu$ or $\mu\nu$ channels. From this we calculate various decay distributions of practical interest for specific choices of decay matrix elements. For the meson decay $Y\to Ke\nu$, we calculate the Ke invariant-mass distribution and all single-particle momentum distributions, transverse to either a plane or a line. We also illustrate properties of the baryon decay $Y\to\Lambda e\nu$.

For a quantitative discussion of the neutrino-induced dilepton events, we adopt the current-fragmentation quark-parton model[5,6] for Y-meson production, and consider plausible models for Y semileptonic decay. We also calculate the effect of transverse Y momentum in broadening decay distributions. By comparing with the experimental transverse-momentum distributions of the slow muon in dimuon events,[1] we obtain the Y-meson mass. The true dimuon rate is estimated to be 2–3 times larger than the observed rate because of the experimental acceptance cutoff at low muon energy. We also make predictions for comparison with future distributions from μ^-e^+ neutrino-induced events in bubble chambers.

II. SEMILEPTONIC DECAY FORMALISM

We consider the semileptonic decay process

$$Y \to l^+ \nu X\,, \tag{1}$$

where X can be any single-particle or multiparticle system, and l^+ denotes e^+ or μ^+. We work always in the approximation of zero e, μ, and ν masses. Particle Y can be a meson, baryon, or heavy lepton of arbitrary spin; for example, Y could be a charmed meson or baryon ground state. The decay matrix element has the form

$$A = \bar{u}_\nu \gamma_\mu (1+\gamma_5)\, v_l \langle X | J_\mu^+ | Y\rangle\,. \tag{2}$$

For unpolarized Y, the relative decay rate has the form

$$dN = L_{\alpha\beta} W_{\alpha\beta} \frac{d^3p_l}{E_l} \frac{d^3p_\nu}{E_\nu}\,, \tag{3}$$

where $L_{\alpha\beta}$ and $W_{\alpha\beta}$ are tensors for the $l\nu$ vertex and the YX vertex, respectively, obtained from averaging over initial spins and summing over final spins and final momenta within the X system. The explicit form of the $L_{\alpha\beta}$ tensor is

$$L_{\alpha\beta} = p_{l\alpha}p_{\nu\beta} + p_{\nu\alpha}p_{l\beta} - \delta_{\alpha\beta}\, p_l\cdot p_\nu - \epsilon_{\alpha\beta\gamma\delta}\, p_{l\gamma}\, p_{\nu\delta}\,. \tag{4}$$

We use the metric $a\cdot b = \vec{a}\cdot\vec{b} - a_0 b_0$. We label the Y momentum by $p_Y = p$ and define the momentum transfer $q=-p_l-p_\nu=p_X-p$. The general form of the $W_{\alpha\beta}$ tensor is then

$$W_{\alpha\beta}=\delta_{\alpha\beta}W_1+\frac{1}{m_Y^2}p_\alpha p_\beta W_2+\frac{1}{2m_Y^2}\epsilon_{\alpha\beta\gamma\delta}p_\gamma q_\delta W_3+\frac{1}{m_Y^2}q_\alpha q_\beta W_4+\frac{1}{2m_Y^2}(p_\alpha q_\beta+q_\alpha p_\beta)W_5\,, \tag{5}$$

in close analogy to the formalism of inelastic lepton scattering.[7] The structure functions W_i depend only on the variables q^2 and $q\cdot p$. In the zero-lepton-mass approximation, the W_4 and W_5 contributions to dN vanish and we obtain

$$L_{\alpha\beta}W_{\alpha\beta}=-2p_l\cdot p_\nu W_1+[2(p_l\cdot p)(p_\nu\cdot p)/m_Y^2+p_l\cdot p_\nu]W_2+[(p_l\cdot q)(p_\nu\cdot p)/m_Y^2-(p_l\cdot p)(p_\nu\cdot q)/m_Y^2]W_3\,. \tag{6}$$

Equation (6) gives the most general allowed dependence of the decay distributions on the leptonic momenta p_l, p_ν. We limit our explicit illustrations to two- and three-particle final states, but the formalism above applies equally to inclusive or exclusive multiparticle channels.

III. TWO-BODY LEPTONIC DECAYS: $Y\to l\nu$

For two-body decays of unpolarized Y particles, the distribution reduces to the trivial form

$$E_l\frac{dN}{d^3p_l}=\delta(m_Y^2+q^2)=\delta(m_Y^2+2p_l\cdot p_Y) \tag{7}$$

up to a constant normalization factor.

Interesting lepton observables are the energy E_l and the momentum transverse to a plane $p_{\perp l}$ or transverse to a line p_{tl}. When the plane or the line includes the Y momentum vector, these transverse-momentum distributions are invariant under the Lorentz transformation from the laboratory to the Y rest frame, and are given by

$$dN/dp_{\perp l}=\pi/m_Y\,, \tag{8}$$

$$dN/dp_{tl}=2\pi p_{tl}/[m_Y(m_Y^2-4p_t^2)^{1/2}]\,, \tag{9}$$

where $0\leq(|p_{\perp l}|,p_{tl})\leq m_Y/2$. The lepton energy distribution is given by

$$dN/dE_l=\begin{cases}\pi\delta(E_l-m_Y/2) & \text{for } E_Y=m_Y\,,\\ \pi/p_Y & \text{for } E_Y>m_Y\,,\end{cases} \tag{10}$$

where $(E_Y-p_Y)/2\leq E_l\leq(E_Y+p_Y)/2$.

IV. THREE-BODY SEMILEPTONIC DECAYS: Y_{l3}

In this section we treat $Y\to l^+\nu X$ with X a single particle. The $W_{\mu\nu}$ tensor takes the form

$$W_{\mu\nu}=\tilde W_{\mu\nu}\delta^4(p-p_l-p_\nu-p_X)\frac{d^3p_X}{E_X}\,, \tag{11}$$

where $\tilde W_{\mu\nu}$ has a representation in terms of $\tilde W_i$ analogous to Eq. (5).

The invariant single-particle distributions have the general form

$$E_i\frac{dN}{d^3p_i}=g_i(s_{jk})\,, \tag{12}$$

where i,j,k are any permutation of l,ν,X, and

$$s_{jk}=-(p_j+p_k)^2 \tag{13}$$

is the invariant jk mass squared. The functions $g_i(s)$ are given by

$$g_i=\int L_{\alpha\beta}\tilde W_{\alpha\beta}\delta^4(p-p_l-p_\nu-p_X)\frac{d^3p_j}{E_j}\frac{d^3p_k}{E_k}\,. \tag{14}$$

General expressions for $p_\perp$, p_t, and E distributions, in terms of the functions g_i, are given in Appendix A. Explicit forms of g_i are also given there for some simple cases of immediate practical interest, namely $\tilde W_1, \tilde W_2, \tilde W_3$ all constant, and $\tilde W_1=-p\cdot(p+q)$.

Although our formalism permits a general discussion of Y_{l3} decays, specific Lagrangian models provide a useful quide to what forms of $\tilde W_{\mu\nu}$ are most reasonable. We therefore consider the following models (see Appendix B for detailed forms of the corresponding decay distributions).

Model I: $Y\to Ke\nu$. The existence of $\mu^-e^+K_S^0$ neutrino events[3,4] motivates us to consider first the mode $Y^+\to\bar K^0e^+\nu$, closely analogous to K_{e3} decay. For a spin-0 Y meson, with no hadronic form factor q^2 dependence, the $\tilde W_i$ are given by

$$\tilde W_2=\text{constant},\quad \tilde W_1=\tilde W_3=0\,. \tag{15}$$

The corresponding forms of $g_i(s)$ for this and subsequent models are given in Appendix B.

Model II: $V-A$ quark decay. In the charm scheme,[8] the favored charm-quark decay mode is $c\to\lambda l\nu$, with $V-A$ couplings, which could be the mechanism underlying $Y\to Xl\nu$ decay. If Y is heavy, the free-quark decay of c might well simulate the inclusive semileptonic decay process, as advocated by Sehgal and Zerwas.[6] Our simplistic approach is to use the free-quark decay matrix, but assign physical masses m_Y and m_X to c and λ quarks, respectively, to ensure correct kinematic bounds for observables (the m_X mass constraint was ignored in Ref. 6). In this model the $\tilde W_i$ are given within an overall normalization by

$$\tilde W_1=-p^2-p\cdot q\,,\qquad \tilde W_2=\tilde W_3=2m_Y^2\,. \tag{16}$$

We can take this model as a prototype for a wide variety of decay processes, e.g., for mesons $Y \to Kl\nu, K^*l\nu, \phi l\nu$ with Y of almost any spin, and for baryons $Y \to \Lambda l\nu$, $\Sigma l\nu$, etc. However, it does not satisfy the special constraints of spin-0→spin-0 decay, incorporated in model I.

Model III: V+A quark decay. Recent theoretical speculations[9] introduce $V+A$ weak currents with one or more new quarks. To represent this possibility, we again use quark decay but with a $V+A$ interaction at the quark vertex.[6] This gives the same $\tilde{W}_i$ as in Eq. (16), except that $\tilde{W}_3$ has opposite sign.

Model IV: vector-meson decay. Diffractive production of new spin-1 mesons could provide a clear experimental signal, with little or no excitation of the nucleon target. For this reason it is interesting to consider separately the decay $Y \to Kl\nu$ with Y of spin 1. The minimal hadronic matrix element $\langle X | J_\mu^+ | Y \rangle = \epsilon_\mu$ leads to the constant structure functions

$$\tilde{W}_1 = 1, \quad \tilde{W}_2 = 1, \quad \tilde{W}_3 = 0. \tag{17}$$

This model might equally well be used for $Y \to K^* e\nu$, with spin-0 Y and spin-1 K^* (or ϕ, etc.), replacing $\tilde{W}_2$ by M_Y^2/M_X^2.

It is interesting to note the parallels with inelastic lepton scattering properties. In model I, the condition $\tilde{W}_1 = 0$ is equivalent to the Callan-Gross relation[10] for a spinless target. In models II and III, the condition $2m_Y^2\tilde{W}_1 = -p\cdot(p+q)\tilde{W}_2$ corresponds to the Callan-Gross relation for a spin-$\frac{1}{2}$ parton carrying the full momentum; the relations $\tilde{W}_2 = \pm\tilde{W}_3$ correspond to familiar quark-parton model results with no antiquarks, for $V \mp A$ couplings.

V. MODEL CALCULATIONS OF THREE-PARTICLE DECAY DISTRIBUTIONS

For the purpose of later comparisons with experiment, we have evaluated the observable distributions for models I–III, with various choices of m_Y and m_X. We discuss each observable in turn. The relevant equations are tabulated in Appendixes A and B.

$p_{\perp l}$ distribution. This is the electron (or muon) momentum transverse to any plane containing the Y momentum vector. Figures 1–3 show $dN/dp_{\perp l}$ for various cases of physical interest: (a) $Y \to Kl\nu$ with $m_Y = 2$ and 4 GeV; (b) $Y \to K^*l\nu$ with $m_Y = 2$ and $m_{K^*} = 0.89$; (c) $Y \to \Lambda l\nu$ with $m_Y = 2.425$ corresponding to the particle mass reported in Ref. 11.

These figures illustrate the following observations.

(i) Three-body decay peaks at small $p_{\perp l}$, in marked contrast to the rectangular distribution of two-body decay: See Eq. (8).

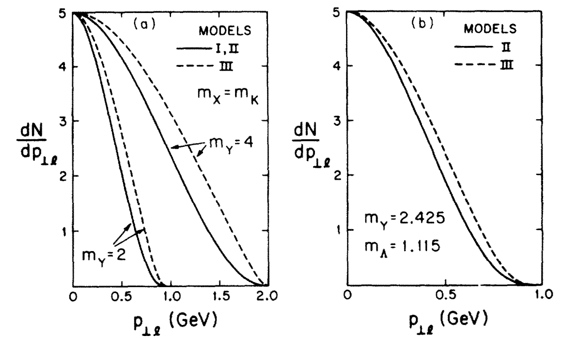

FIG. 1. Lepton momentum distribution $dN/dp_{\perp l}$ transverse to a plane, for the cases (a) Y-meson decay $Y \to Kl\nu$ with $m_Y = 2$ and 4 GeV and $m_K = 0.495$. (b) Y-baryon decay $Y \to \Lambda l\nu$ with $m_Y = 2.425$ and $m_\Lambda = 1.115$. Solid lines for models I and II, dashed lines for model III.

(ii) There is some model dependence in the shape, but very high experimental statistics are required to resolve the differences between models, if the masses are unknown *a priori*. Models I and II give identical $p_{\perp l}$ predictions.

(iii) The end point of the distribution is

$$p_\perp(\max) = (m_Y^2 - m_X^2)/(2m_Y). \tag{18}$$

To a first approximation the overall shape of the distribution, within a given model, is controlled by this parameter also. Therefore, if the identity of X is unknown (e.g., K, K^*, etc.), the quantity determined by fitting an experimental distribution is not directly m_Y but rather $m_Y - m_X^2/m_Y$.

(iv) If more than one Y particle with different quantum numbers is present, the superposition of $p_\perp$ distributions will look quite different from a single-particle case, if the Y masses differ sufficiently, as illustrated in Fig. 3.

From an experimental distribution, the average value $\langle p_\perp \rangle$ is better determined than the end point $p_\perp(\max)$. In the models we have studied, $\langle p_{\perp l} \rangle$ can be empirically related to m_Y (for a given m_X) by a

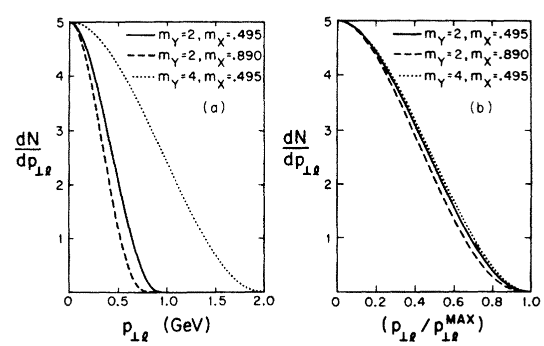

FIG. 2. Comparison of shapes of $dN/dp_{\perp l}$ distributions for Y-meson decays in model I, with $m_Y = 2$ and 4 GeV, $m_X = 0.495$ (K) and 0.890 (K^*), plotted versus (a) $p_\perp$ and (b) $p_\perp/p_\perp(\max)$.

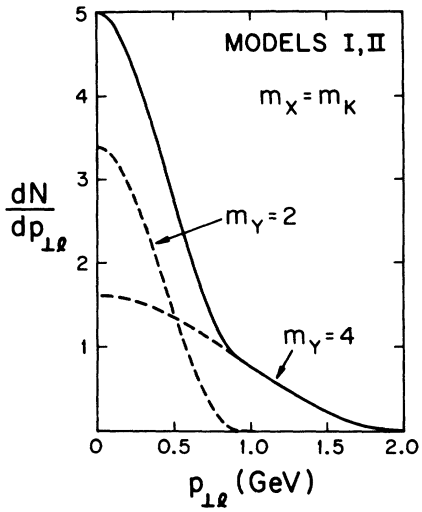

FIG. 3. Superposition of $dN/dp_{\perp l}$ distributions for two Y mesons ($m_Y = 2$ GeV and $m_Y = 4$) with different quantum numbers decaying into $K l \nu$.

linear formula

$$\langle p_{\perp l}\rangle = a + b m_Y \,. \tag{19}$$

The coefficients a and b are given in Table I for the cases $m_X = 0.495$ (K) and $m_X = 0.890$ (K^*). Hence from an experimental value of $\langle p_{\perp l}\rangle$ we deduce

$$m_Y = (\langle p_{\perp l}\rangle - a)/b \,. \tag{20}$$

A similar relation holds for mean values of other distributions, and the corresponding model values of a and b are also listed in Table I.

We use this approach to estimate m_Y from the $p_{\perp l}$ distributions of the slow muon in dimuon events,[1] measured transverse to the plane defined by the incident neutrino and the fast muon. According to the current-fragmentation parton

TABLE I. Coefficients for empirical mean-value formula $\langle O\rangle = a + b m_Y$, fitted to the range $1.5 \le m_Y \le 5$ GeV, for cases $m_X = 0.495$ (K) and $m_X = 0.890$ (K^*).

Observable $\langle O\rangle$	a	b	X, model
$\langle p_{\perp l}\rangle$	−0.037	0.154	K I, II
	−0.054	0.181	K III
	−0.100	0.161	K^* I, II
	−0.134	0.189	K^* III
$\langle p_{tl}\rangle$	0.001	0.169	K I, II
	−0.039	0.173	K III
	−0.064	0.178	K^* I, II
	−0.059	0.175	K^* III
$\langle p_{\perp K}\rangle$	−0.025	0.204	K I
	−0.021	0.178	K II, III
$\langle p_{tK}\rangle$	−0.097	0.183	K I
	−0.116	0.188	K II, III
$\langle m_{Kl}\rangle$	0.133	0.593	K I, III
	0.229	0.484	K II

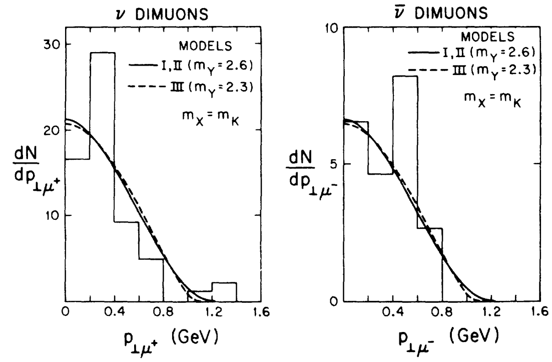

FIG. 4. Slow-muon $p_\perp$ distributions from ν and $\bar{\nu}$ dimuon events, compared with models I, II ($m_Y = 2.6$) GeV, and model III ($m_Y = 2.3$).

model, the Y momentum vector lies in this plane: See Sec. VI. The value $\langle p_{\perp\mu^+}\rangle = 0.35$ from neutrino dimuons[1] leads to the estimates $m_Y = 2.6$ for models I, II and $m_Y = 2.3$ for model III. Figure 4 shows a comparison with the slow-muon $p_\perp$ distributions for ν and $\bar{\nu}$ dimuons. These estimates take no account of broadening of the distribution due to experimental resolution or transverse motion of Y, and hence can be regarded as upper limits on the true mass. We make a quantitative study of broadening due to $p_{\perp Y}$ in Sec. VII.

$p_{\perp\nu}$ distribution. Experimentally $p_{\perp\nu}$ can be deduced from the other two decay particles:

$$p_{\perp\nu} = -(p_{\perp l} + p_{\perp X}) \,. \tag{21}$$

For our models I–III, the predictions for $p_{\perp\nu}$ and $p_{\perp l}$ are related as follows:

$$\begin{aligned} &p_{\perp\nu}(\mathrm{I}) = p_{\perp\nu}(\mathrm{III}) = p_{\perp l}(\mathrm{I}) \,, \\ &p_{\perp\nu}(\mathrm{II}) = p_{\perp l}(\mathrm{III}) \,. \end{aligned} \tag{22}$$

The remarks about $p_{\perp l}$ distributions above apply here also.

$p_{\perp X}$ distributions. In this case the only single identifiable particle X of current practical interest is the kaon. Figure 5 shows $dN/dp_{\perp K}$ for the same physical cases as studied above for the lepton

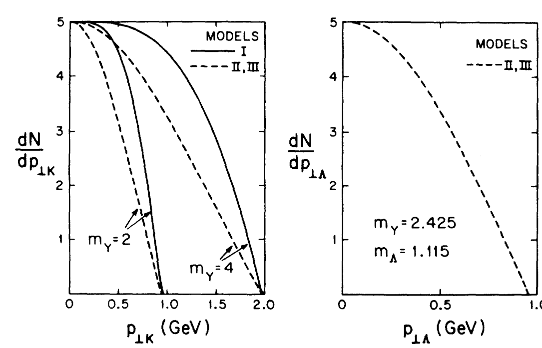

FIG. 5. K, Λ momentum distributions transverse to a plane, for the same physical cases as in Fig. 1.

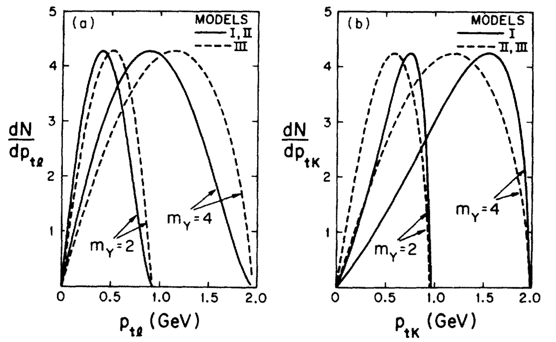

FIG. 6. Momentum distributions dN/dp_t transverse to a line, for $Y \to Kl\nu$ decays with $m_Y = 2$. (a) Lepton distribution, solid line for models I or II, dashed line for model III. (b) Kaon distribution, solid line for model I, dashed line for models II or III.

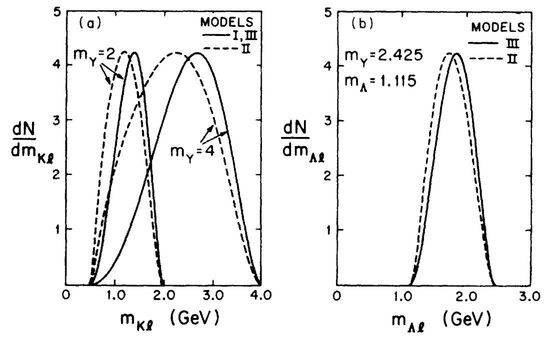

FIG. 8. Distributions of invariant mass (a) m_{Kl} for $Y \to Kl\nu$ with $m_Y = 2$ and 4 GeV. (b) $m_{\Lambda l}$ for $Y \to \Lambda l\nu$ with $m_Y = 2.425$. Solid curves for models I or III, dashed curves for model II.

distributions. The model dependence of $p_{\perp K}$ is more marked, but otherwise our general discussion of $p_{\perp l}$ applies equally here. Since the $V-A$ interference amplitude $\tilde{W}_3$ never contributes to $p_{\perp K}$ [see Eq. (A23)], there is no difference between the $p_{\perp K}$ predictions of models II and III. The mean value $\langle p_{\perp K}\rangle$ can be approximated as in Eq. (19); the coefficients are given in Table I.

p_{tl} *distributions.* This is the lepton momentum transverse to a line, containing the Y momentum vector, and is invariant under a Lorentz transformation to the Y rest frame. Figure 6 shows dN/dp_{tl} for $Y \to Kl\nu$ with $m_Y = 2$. The maximum value is again given by Eq. (18). The mean value $\langle p_{tl}\rangle$ can again be approximated as in Eq. (19); the coefficients are found in Table I.

$p_{t\nu}$ *distributions.* The relation to p_{tl} cases is similar to Eq. (22).

p_{tK} *distributions.* Examples are shown in Fig. 6. The mean values can be approximated as in Eq. (19), with coefficients given in Table I.

E distributions. These depend on the initial Y momentum. Figure 7 illustrates typical features of the p_Y momentum dependence of E_l. To make contact with experiment we need a dynamical model of Y production; this is taken up in Sec. VI.

m_{lX} *distributions.* The invariant mass m_{lX} of the lX system can be measured in meson decays such as $Y \to Kl\nu$ or baryon decays such as $Y \to \Lambda l\nu$. Since m_{lX} is a Lorentz invariant, predictions for this distribution are independent of the Y momentum and hence independent of the Y production mechanism. Possible practical limitations on the use of this distribution are the identification of X as coming from the Y decay and of the decay as being three-body. Figure 8 shows m_{Kl} and $m_{\Lambda l}$ distributions from assumed $Y \to Kl\nu$ and $Y \to \Lambda l\nu$ decays. The $Kl\nu$ case is for $m_Y = 2$ and 4 GeV; the $\Lambda l\nu$ case is again calculated with $m_Y = 2.425$.

For the $Y \to Kl\nu$ case, the average values are

$$\begin{aligned} \langle m_{Kl}\rangle &= 0.133 + 0.593 m_Y, \quad \text{models I, III} \\ \langle m_{Kl}\rangle &= 0.229 + 0.484 m_Y, \quad \text{model II} \end{aligned} \tag{23}$$

for $1.5 < m_Y < 5$ GeV. This result differs somewhat from the crude estimate $m_Y = \sqrt{3}\langle m_{Kl}\rangle$, based on energy equipartition.

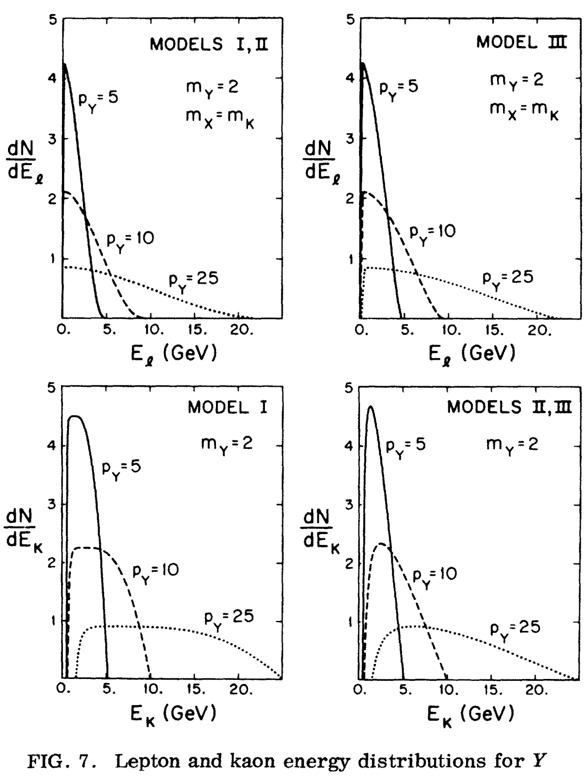

FIG. 7. Lepton and kaon energy distributions for $Y \to Kl\nu$ with $m_Y = 2$ GeV and the choices $p_Y = 5$, 10, 25.

VI. PARTON MODEL FOR Y PRODUCTION IN CURRENT-FRAGMENTATION REGION

A model for the Y-production mechanism is needed before we can compare our decay distributions with experiment. In order to compare with $p_\perp$ or p_t decay distributions, we need to know which planes or which line the Y momentum vector lies in; to calculate E distributions of decay particles we need the E_Y distribution.

In this paper we focus our attention on Y-particle production in neutrino and antineutrino experiments. We adopt the quark-parton model ansatz for Y-meson production in the current-fragmentation region,[5] namely,

$$\frac{d\sigma^Y}{dx\,dy\,dz}=\frac{d\sigma^Q}{dx\,dy}D(z), \tag{24}$$

where $d\sigma^Q/dx\,dy$ is the cross section for production of a new quark Q with energy ν, and $D(z)$ is the probability that Y is a fragment of Q with energy $z\nu$. The scaling variables are

$$\begin{aligned} x&=Q^2/(2M\nu),\\ y&=\nu/E,\\ z&=E_Y/\nu, \end{aligned} \tag{25}$$

where E is the incident neutrino energy, while ν and Q^2 are the lab energy and the invariant momentum transfer squared transmitted by the current, respectively.

For our subsequent calculations we take the standard 4-quark model[8] with Q as the charm quark, so that[12,13]

$$\frac{d\sigma^Q}{dx\,dy}=\frac{G^2ME}{\pi}[xy+x'(1-y)] \times[N_{\rm sea}(x')+\sin^2\theta_C N_{\rm val}(x')]\theta(W-W_{\rm th}). \tag{26}$$

Here $N_{\rm sea}$ and $N_{\rm val}$ are sea- and valence-quark distributions, $W^2=2MEy(1-x)+M^2$ is the invariant hadron mass squared, and $W_{\rm th}\geq m_Y+M$ is the charm threshold. The variable x' can either be chosen to equal x (fast rescaling), or chosen to give slow rescaling, for example[13,14]

$$x'=(Q^2+m_Q{}^2)/(2M\nu)=x+m_Q{}^2/(2MEy), \tag{27}$$

where m_Q is the charm-quark mass. With fast rescaling, an effective $W_{\rm th}$ is chosen some way above the lowest physical threshold.[12] The calculations illustrated in this paper are based on the fast-rescaling parameterization of Ref. 12, with $W_{\rm th}=4$. We have checked that the slow-rescaling parameterization of Ref. 13 with $m_Q=1.5$ leads to essentially the same results for the Y-production spectrum $d\sigma/dE_Y$,

$$\frac{d\sigma}{dE_Y}=\int\phi(E)dE\int dx\,dy\,\frac{1}{Ey}\frac{d\sigma^Q}{dx\,dy}D(z=E_Y/(yE)), \tag{28}$$

where $\phi(E)$ is the incident neutrino spectrum. For comparison with neutrino dimuon events, we use the spectrum of Ref. 1.

The fragmentation function $D(z)$ is expected to behave like z^{-1} at small z. The experimental neutrino and electron deep-inelastic data[15-17] for hadron fragments (mainly pions and kaons) are consistent with a behavior[6]

$$D(z)=C(1-z)/z, \tag{29}$$

at least for $z>0.1$, as shown in Fig. 9. Here C is an unknown constant. Since $D(z)$ for Y particles is unknown, we also considered some other extreme possibilities, namely $D(z)=1/z$ and $D(z)=(1+1/z)$, but found very little difference in the final E_t spectrum. Consequently, we restrict our attention to Eq. (29).

The current-fragmentation picture is not expected to apply at very small z. In our calculations we impose a lower bound $z\geq z_0$, with z_0 in the range 0.1–0.2. The results are not too sensitive to the precise choice of z_0 relative to the present experimental uncertainties.

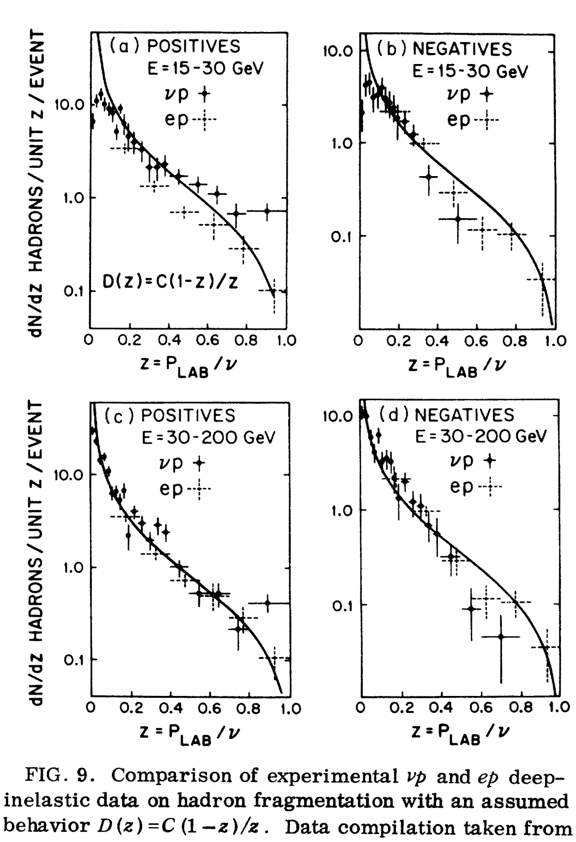

FIG. 9. Comparison of experimental νp and ep deep-inelastic data on hadron fragmentation with an assumed behavior $D(z)=C(1-z)/z$. Data compilation taken from Ref. 15.

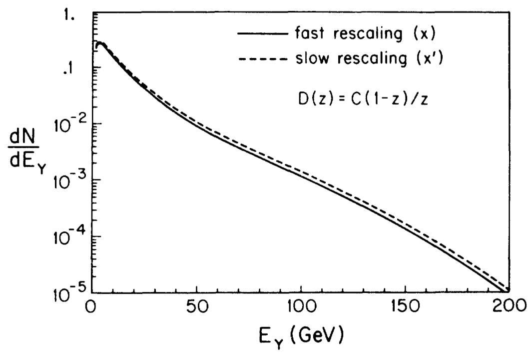

FIG. 10. The Y-production spectrum dN/dE_Y calculated with the ν spectrum of Ref. 1, for $D(z)=(1-z)/z$ and $z_0=0.1$. Solid curve is fast rescaling result; dashed curve shows slow rescaling with the x' variable of Eq. (27).

Figure 10 shows the Y-production spectrum for both fast- and slow-rescaling assumptions, which give remarkably similar results. The spectrum peaks near $E_Y=5$ GeV.

The E_l distribution from Y decay is given by

$$\frac{dN}{dE_l}=\int dE\,\phi(E)\int dx\,dy\,dz\frac{d\sigma^Q}{dx\,dy}D(z)\frac{dN}{dE_l}(E_Y=yzE), \tag{30}$$

where the expression for $(dN/dE_l)(E_Y)$ at given E_Y is given in Eq. (A3). A similar form holds for dN/dE_K. Technical details of the integration are described in Appendix C.

Figure 11 shows the E_l distribution from $Y\to Kl\nu$, for model I with the choices $m_Y=2$ and 4, and thresholds $W_{th}=4$ and 6, respectively. The slow-muon distribution from the neutrino-induced dimuon events of Ref. 1 is shown for comparison. Our studies show that the lepton spectrum dN/dE_l is dominated by the incident neutrino spectrum and the fragmentation function $D(z)$: This distribution is not sensitive to the Y mass, and cannot be used to determine m_Y. The effect of changing m_Y is hard to distinguish from the effect of changing z_0.

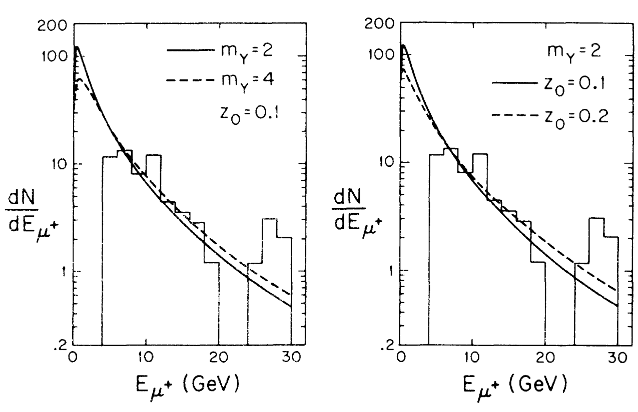

FIG. 11. Slow-muon energy distribution dN/dE_l for model I, calculated with the neutrino spectrum of Ref. 1: (a) for $z_0=0.1$, $m_Y=2$ and 4 GeV (solid and dashed lines, respectively); (b) for $m_Y=2$, $z_0=0.1$ and 0.2 (solid and dashed lines, respectively). The μ^+ distribution from the neutrino dimuon events of Ref. 1 is shown for comparison.

However, the shape of the E_l distribution is very important in determining the net cross section for Y production from experiment. The spectrum peaks at very low values around $E_l=1$ GeV, where the acceptance of the dimuon experiment goes to zero. For $m_Y=2$ and $z_0=0.1-0.2$, the predicted fraction of events above the experimental acceptance cutoff at $E_\mu\simeq 4$ GeV is

$$N(E>4)/N(\text{all } E)=0.3-0.4 \tag{31}$$

with the neutrino spectrum of Ref. 1. Assuming that our three-body decay models approximate the physical decay mechanism, and that our Y-production model is reasonable, Eq. (31) indicates that the observed ratio of dimuon to single-muon events[1] for $E>30$ GeV,

$$(\sigma_{\mu\mu}/\sigma_\mu)(\text{experimental})\simeq(0.8\pm0.3)\times10^{-2}, \tag{32}$$

reflects a true ratio,

$$(\sigma_{\mu\mu}/\sigma_\mu)(\text{true})\simeq(2.4\pm1.2)\times10^{-2}. \tag{33}$$

Calculations[12] with the standard 4-quark charm model require a mean muonic branching ratio B_μ of charmed particles of order $B_\mu\simeq10\%$ to account for the experimental dimuon rate Eq. (32). Equation (33) indicates values $B_\mu\simeq15-40\%$ instead. This is to be compared with the theoretical estimate $B_\mu\simeq20\%$ from equal couplings to quarks and leptons[18] and the upper bound $B_\mu\leq50\%$ for purely semileptonic decay with μ-e universality. However, models with enhanced charm production, or with more than one new quark,[9] require smaller branching ratios.[12]

We expect the μ^-e^+ events[3,4] to have the same Y-particle origin and branching ratio as the ν-induced $\mu^-\mu^+$ events.[1,2] Within our model we can then use the $\mu^-\mu^+$ rate to predict the μ^-e^+ rate for the neutrino spectrum of the Fermilab bubble-chamber experiment. For the same angular acceptance as the dimuon experiment, we calculate from Eq. (32) a total μe rate for $E>30$ GeV of

$$(\sigma_{\mu e}/\sigma_\mu)(\text{Fermilab Expt. No. E.28A})=(2.2\pm1.1)\times10^{-2}. \tag{34}$$

VII. DISTRIBUTION BROADENING FROM Y TRANSVERSE MOMENTUM

The current-fragmentation parton model of Sec. VI assumes that Y particles are produced exactly along the axis of momentum transfer $\vec{q}$. Although the dominance of longitudinal momenta is a common feature of hadron production, there is also a spread of momenta p_t transverse to the longitudinal axis, which is approximately independent of the longitudinal momentum. Thus we expect that a more correct description of Y production would be given by

$$\frac{d\sigma}{dp_{LY}dp_{tY}^2}=f(p_{LY})h(p_t^2), \tag{35}$$

where p_L is the longitudinal Y momentum, $f(p_L)$ is given by the current-fragmentation model as before, and $h(p_t^2)$ is an empirical p_t dependence

$$h(p_t^2)=b\exp(-bp_t^2). \tag{36}$$

For inclusive ρ and ω production by hadrons, the experimental value is $b\simeq 6$ GeV^{-2}, whereas $b\simeq 1.3$ GeV^{-2} for inclusive ψ production.[19] For inclusive hadron production by neutrinos, a value $b\simeq 4.1$ GeV^{-2} is measured.[15] We do not know what value of b to assume for Y production, but if it depends primarily on the mass of the produced particle, we would expect a value somewhere between $b=1$ and $b=6$ GeV^{-2}.

The practical effect of this added p_{tY} dependence is to smear and broaden the predicted $p_\perp$ and p_t distributions somewhat. The m_{lK} distributions are absolutely unaffected. The E distributions too are unchanged, neglecting p_{tY}^2 compared to E_Y^2. We illustrate this broadening effect for the $p_\perp$ distributions below.

We consider $p_{\perp l}$ distributions transverse to a plane containing the initial neutrino and fast final μ^-. The longitudinal axis $\vec{q}$ of Y production in our model lies in this plane, and both $p_{\perp l}$ and $p_{\perp Y}$ are invariant under any Lorentz boost in this plane. For each initial Y momentum, we can therefore make a Lorentz transformation without altering $p_\perp$ to a frame where Y has only its original transverse-momentum component $p_{\perp Y}$, with distribution

$$dN/dp_{\perp Y}=\exp(-b_{\perp Y}^2) \tag{37}$$

up to an overall normalization. The resulting smeared $p_{\perp l}$ distribution obtained from Eq. (12) is

$$\frac{dN}{dp_{\perp l}}=\int\frac{dp_{\perp Y}\exp(-bp_{\perp Y}^2)}{(m_Y^2+p_{\perp Y}^2)^{1/2}}\int ds\, g_l(s), \tag{38}$$

where the integration limits are

$$s(\min)=m_X^2, \quad s(\max)=m_Y^2-2p_{\perp l}(p_{\perp Y}^2+m_Y^2)^{1/2}+2p_{\perp l}p_{\perp Y}, \tag{39}$$

$$p_{\perp Y}(\min)=(p_{\perp l}^2-\alpha^2 m_Y^2)/(2\alpha p_{\perp l}), \quad p_{\perp Y}(\max)=\infty, \tag{40}$$

where $\alpha=(m_Y^2-m_X^2)/(2m_Y^2)$. The formula for $p_{\perp\nu}$ is similar. The expression for $p_{\perp X}$ is the same as Eq. (38) but with $g_X(s)$ in place of $g_l(s)$ and with

$$s(\min)=0, \quad s(\max)=m_Y^2+m_X^2+2p_{\perp Y}p_{\perp X}-2(p_{\perp Y}^2+m_Y^2)^{1/2}(p_{\perp X}^2+m_X^2)^{1/2}, \tag{41}$$

$$p_{\perp Y}(\min)=\beta p_{\perp X}-\gamma(p_{\perp K}^2+m_X^2)^{1/2}, \quad p_{\perp Y}(\max)=\beta p_{\perp X}+\gamma(p_{\perp X}^2+m_X^2)^{1/2}, \tag{42}$$

where $\beta=(m_Y^2+m_X^2)/(2m_X^2)$ and $\gamma=(m_Y^2-m_X^2)/(2m_X^2)$. The expressions for smeared p_t distributions (transverse to the $\vec{q}$ axis) are more complicated and will not be given here.

The case of two-body decay is reached by taking $m_X=0$ and $g(s)=\delta(s)$; cf. Eq. (7). In Eq. (38) the integral $\int g(s)ds$ is 1, and the $p_{\perp Y}$ limits become

$$p_{\perp Y}(\min)=(4p_{\perp l}^2-m_Y^2)/(4p_{\perp l}), \quad p_{\perp Y}(\max)=\infty. \tag{43}$$

Quantitative calculations of spectrum broadening, based on Eq. (38), are illustrated in Figs. 12–14. An important feature of the results is that the changes in shape due to smearing are relatively minor, even for such a wide p_{tY} distribution as the extreme $b=1$ case. The principal modification is the extension of the tails of the distributions to higher $p_\perp$. Our exact method and calculations bear little resemblance to the claimed approximation and results of Ref. 20.

For the three-body model, the peak width at mid-height is almost unchanged. Qualitatively this can be understood as follows: At intermediate $p_{\perp l}$ values, the enhancement from Y particles moving parallel to the lepton momentum is offset

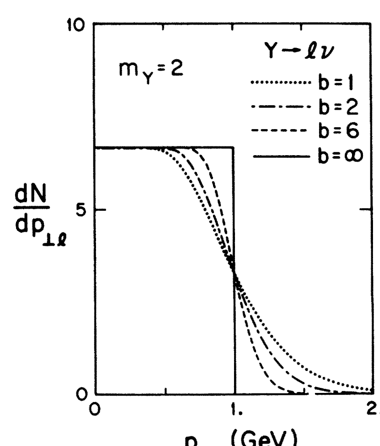

FIG. 12. Broadening of $p_{\perp l}$ distribution in $Y\to l\nu$ decay due to Y transverse momentum, with $m_Y=2$ GeV and smearing parameter values $b=1,2,6,\infty$.

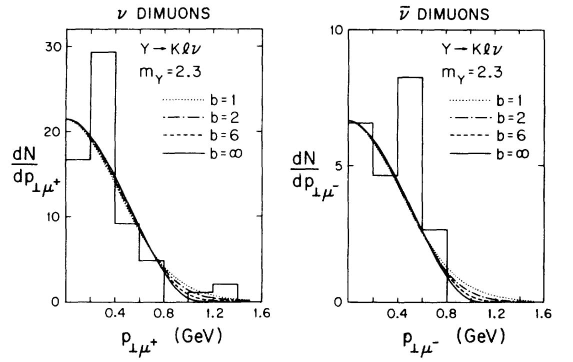

FIG. 13. Broadening of $p_{\perp l}$ distribution in $Y \rightarrow Kl\nu$ decay for model I with $m_Y = 2.3$ GeV and smearing parameter $b = 1, 2, 6, \infty$ (dotted, dash-dotted, dashed, and solid curves, respectively). For comparison the slow-muon distributions from the ν and $\bar{\nu}$ dimuon events of Ref. 1 are shown.

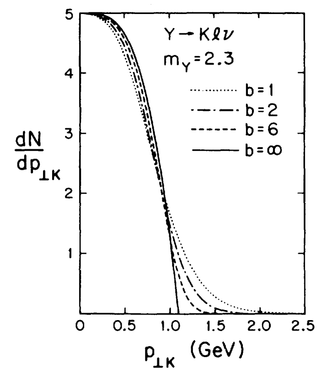

FIG. 14. Broadening of $p_{\perp K}$ distributions in $Y \rightarrow Kl\nu$ decays for model I with $m_Y = 2.3$ GeV and smearing parameters $b = 1, 2, 6, \infty$ (dotted, dash-dotted, dashed, and solid curves, respectively).

by a depletion from Y particles moving antiparallel.

The broadening effect is somewhat stronger for the kaon distribution, but is still not a big correction. Because of its large mass the kaon moves more slowly in the Y rest frame, and is therefore more affected by the $p_{\perp Y}$ Lorentz boost.

We conclude that distortions from the Y rest frame $p_{\perp l}$ and $p_{\perp K}$ distributions caused by the transverse Y motion are relatively minor and that ignoring them will not lead to significant Y mass overestimates. The quantitative effect on $\langle p_\perp \rangle$ values for model I with $m_Y = 2$ and $m_X = 0.495(K)$ is illustrated by the following values:

$$\langle p_{\perp e} \rangle = \begin{cases} -0.026 + 0.153 m_Y & \text{for } b = 6 \\ -0.006 + 0.150 m_Y & \text{for } b = 2 \\ \ \ 0.020 + 0.146 m_Y & \text{for } b = 1\,, \end{cases}$$

$$\langle p_{\perp K} \rangle = \begin{cases} -0.003 + 0.200 m_Y & \text{for } b = 6 \\ \ \ 0.038 + 0.193 m_Y & \text{for } b = 2 \\ \ \ 0.086 + 0.187 m_Y & \text{for } b = 1\,. \end{cases}$$

The distribution-broadening approach can also be used to calculate lepton $p_\perp$ distributions from sequential decays. As an illustration, a chain decay mode of pseudoscalar Y particles through the heavy lepton presumably discovered at SPEAR[21] has been suggested[22]:

$$Y^+ \rightarrow U^+ \nu_U, \quad U^+ \rightarrow l^+ \nu_l \bar{\nu}_U\,.$$

The two-body decay of Y has the effect of smearing the subsequent three-body decay of U. The smearing function of Eq. (37) gets replaced by the uniform distribution

$$\frac{dN}{dp_{\perp U}} = \theta(p_{\perp U}(\max) - |p_{\perp U}|)\,, \tag{44}$$

where $p_{\perp U}(\max) = (m_Y^2 - m_U^2)/(2m_Y)$. For typical masses $m_Y = 2.3$ and $m_U = 1.8$, the allowed $p_{\perp U}$ range in Eq. (44) is small, and the resulting $p_{\perp l}$ distribution differs little from that of the decay of a U at rest.

VIII. SUMMARY

We have developed a general formalism for discussing $Y \rightarrow l\nu X$ decays, and have applied it using specific decay modes and matrix elements as follows:

(i) to illustrate the shapes of decay distributions and their dependence on the masses of X and Y;

(ii) to find empirical formulas for average quantities, such as $\langle p_\perp \rangle = a + b m_Y$, for given m_X;

(iii) to estimate the Y-particle mass from $\langle p_\perp \rangle$ for the slow muon in neutrino dimuon events, obtaining $m_Y \simeq 2.3$ GeV.

We use the quark-parton current-fragmentation model for Y production by neutrinos to calculate the E_Y spectrum and the E_l distribution resulting from $Y \rightarrow Kl\nu$ decay. We find the following:

(iv) The shape of dN/dE_l is dominated by the incident neutrino spectrum and the fragmentation function $D(z)$. It is not very sensitive to m_Y and does not provide a good way to determine the latter.

(v) A substantial part of the decay lepton distribution falls below $E_l = 4$ GeV, the lower acceptance limit in the dimuon experiment of Ref. 1. The true dimuon rate may therefore be 2–3 times larger than the rate observed in that experiment.

(vi) The ratio of $\mu^- e^+$ events to single μ^- events in the Fermilab bubble-chamber experiment is estimated to be 2×10^{-2}.

Finally, we use an exact method to calculate the distribution-broadening effect of transverse Y motion. For the likely physical range of Y transverse-momentum spreads we find the following:

(vii) Transverse Y motion adds a tail to $p_\perp$ decay distributions, but otherwise gives rather small corrections.

ACKNOWLEDGMENTS

We thank T. Gottschalk, G. Weller, and E. Braaten for valuable assistance with computations. We thank J. Bjorken, D. Cline, G. Dass, W. Fry, K. Gaemers, K. Geer, F. Halzen, J. Mapp, H. Miettinen, R. Prepost, D. Reeder, P. Tsai, J. Von Krogh, and T. Weiler for discussions.

APPENDIX A: THREE-BODY SEMILEPTONIC DECAY

The observable distributions for $Y \to l\nu X$ decay can be expressed in terms of the functions g_i of Eq. (12):

$$dN/dp_{\perp i} = (\pi/m_Y)\int ds\, g_i(s)\,, \tag{A1}$$

$$dN/dp_{ti} = 2\pi p_{ti}\int ds\, g_i(s)\,[(m_Y^2+m_i^2-s)^2 - 4m_Y^2(p_{ti}^2+m_i^2)]^{-1/2}\,, \tag{A2}$$

$$dN/dE_i = (\pi/p_Y)\int ds\, g_i(s)\,, \tag{A3}$$

$$dN/dm_{lX} = 2\pi m_{lX}(m_Y^2/m_{lX}^2-1)\,g_\nu(m_{lX}^2)\,. \tag{A4}$$

Here m_{lX} is the invariant mass of the lX system. The integration limits on the variable

$$s = -(p_Y-p_i)^2 = m_Y^2+m_i^2-2E_YE_i+2p_Yp_i\cos\theta \tag{A5}$$

are determined from the constraints

$$\begin{aligned} &s \le m_Y^2\,,\\ &s \ge (m_j+m_k)^2\,,\\ &s \le s(\cos\theta=+1)\,,\\ &s \ge s(\cos\theta=-1)\,, \end{aligned} \tag{A6}$$

plus the condition that the quantity ($p_{\perp l}, p_{ti}$, etc.) for which we are computing the distribution is held fixed. The appropriate integration limits for Eqs. (A1)–(A3) are (for positive $p_\perp$)

$p_{\perp l}$ or $p_{\perp\nu}$:

$$\begin{aligned} s_{\min} &= m_X^2\,,\\ s_{\max} &= m_Y^2-2m_Yp_{\perp l}\,, \end{aligned} \tag{A7}$$

$p_{\perp X}$:

$$\begin{aligned} s_{\min} &= 0\,,\\ s_{\max} &= m_X^2+m_Y^2-2m_Y(m_X^2+p_{\perp X}^2)^{1/2}\,, \end{aligned} \tag{A8}$$

E_l:

$$\begin{aligned} s_{\min} &= \max\{m_X^2,\, m_Y^2-2E_l(E_Y+p_Y)\}\,,\\ s_{\max} &= m_Y^2-2E_l(E_Y-p_Y)\,, \end{aligned} \tag{A9}$$

E_X:

$$\begin{aligned} s_{\min} &= \max\{0,\, m_X^2+m_Y^2-2E_XE_Y-2p_Xp_Y\}\,,\\ s_{\max} &= m_X^2+m_Y^2-2E_XE_Y+2p_Xp_Y\,. \end{aligned} \tag{A10}$$

Equations (A7) and (A8) also describe the p_{ti} cases, when p_t is substituted for $p_\perp$.

We note that $dN/dp_{\perp l}$ and dN/dE_l from Eqs. (A1) and (A3) are described by the same basic integral, with different functional forms arising from the different limits of integration (A7) and (A9). If

$$E_l \ge \tfrac{1}{2}(m_Y^2-m_X^2)/(E_Y+p_Y) \tag{A11}$$

the lower limits become identical, and we can write the two distributions in terms of a common function

$$H(\zeta) = \pi\int_{m_X^2}^{m_Y^2(1-\zeta)} ds\, g_l(s) \tag{A12}$$

as

$$dN/dp_{\perp l} = m_Y^{-1}H(2p_{\perp l}/m_Y)\,, \tag{A13}$$

$$dN/dE_l = p_Y^{-1}H(2E_l/(E_Y+p_Y))\,. \tag{A14}$$

An approximate form of this result was stated in Ref. 6. Equation (A14) is strictly valid only for lepton energies satisfying Eq. (A11). Similar equations apply to neutrino distributions. For X distributions an analogous result holds if

$$E_X \ge \tfrac{1}{2}m_Y^{-2}[E_Y(m_Y^2+m_X^2)-p_Y(m_Y^2-m_X^2)]\,. \tag{A15}$$

The corresponding relations are

$$K(\zeta) = \pi\int_0^{m_X^2+m_Y^2(1-\zeta)} ds\, g_X(s)\,, \tag{A16}$$

$$dN/dp_{\perp X} = m_Y^{-1}K(2(p_{\perp X}^2+m_X^2)^{1/2}/m_Y)\,, \tag{A17}$$

$$dN/dE_X = p_Y^{-1}K(2(E_XE_Y-p_Xp_Y)/m_Y^2)\,. \tag{A18}$$

The complexity in this case comes from the nonvanishing X mass.

The kinematic ranges of $p_\perp$ and p_t are the same for l, ν, and X, namely

$$\begin{aligned} &p_t(\min) = 0\,,\\ &p_\perp(\max) = -p_\perp(\min) = p_t(\max)\\ &\qquad = (m_Y^2-m_X^2)/(2m_Y)\,. \end{aligned} \tag{A19}$$

The limits for the other variables are as follows:

$$\begin{aligned} &E_l(\min) = 0\,,\\ &E_l(\max) = (m_Y^2-m_X^2)(E_Y+p_Y)/(2m_Y^2)\,, \end{aligned} \tag{A20}$$

$$E_X(\min)=\begin{cases} m_X \text{ for } E_Y \le (m_X{}^2+m_Y{}^2)/(2m_X), \\ [E_Y(m_Y{}^2+m_X{}^2)-p_Y(m_Y{}^2-m_X{}^2)]/(2m_Y{}^2) \\ \quad \text{for } E_Y \ge (m_X{}^2+m_Y{}^2)/(2m_X), \end{cases} \tag{A21}$$

$$E_X(\max)=[E_Y(m_Y{}^2+m_X{}^2)+p_Y(m_Y{}^2-m_X{}^2)]/(2m_Y{}^2),$$

$$m_{lX}(\min)=m_X, \quad m_{lX}(\max)=m_Y. \tag{A22}$$

For the case that $\tilde{W}_i=$constant, we find

$$g_l(s)=\pi s^{-2}(m_Y{}^2-s)(s-m_X{}^2)^2[\tilde{W}_1+\tilde{W}_2 s/(2m_Y{}^2)+\tilde{W}_3(2m_X{}^2m_Y{}^2+sm_Y{}^2+sm_X{}^2-4s^2)/(12sm_Y{}^2)], \tag{A23}$$

$$g_\nu(s)=g_l(\tilde{W}_3\to-\tilde{W}_3), \tag{A24}$$

$$g_X(s)=2\pi s\tilde{W}_1+\pi\tilde{W}_2[s^2-2s(m_Y{}^2+m_X{}^2)+(m_Y{}^2-m_X{}^2)^2]/(6m_Y{}^2). \tag{A25}$$

In fact this form for $g_X(s)$ holds independent of any assumptions about the $\tilde{W}_i$. The sign change of $\tilde{W}_3$ between Eqs. (A23) and (A24) reflects the fact that $\tilde{W}_3$ is a V-A interference term.

Another case of interest is $\tilde{W}_1=-C_1 p\cdot(p+q)$ with $\tilde{W}_2=\tilde{W}_3=0$, for which

$$g_l(s)=\tfrac{1}{6}\pi C_1 s^{-3}(m_Y{}^2-s)(s-m_X{}^2)^2 \times[2s^2+s(m_X{}^2+m_Y{}^2)+2m_X{}^2m_Y{}^2], \tag{A26}$$

$$g_\nu(s)=g_l(s), \tag{A27}$$

$$g_X(s)=\pi C_1 s(m_X{}^2+m_Y{}^2-s). \tag{A28}$$

APPENDIX B: DECAY FUNCTIONS OF MODELS

The invariant single-particle decay distributions are described in terms of functions $g_i(s_{jk})$: See Eq. (12) and Appendix A. The functional forms of g_i in the models considered are as follows, within overall constants.

Model I.

$$g_l(s)=s^{-1}(m_Y{}^2-s)(s-m_X{}^2)^2\equiv g_1(s), \tag{B1}$$

$$g_\nu(s)=g_l(s), \tag{B2}$$

$$g_X(s)=s^2-2s(m_Y{}^2+m_X{}^2)+(m_Y{}^2-m_X{}^2)^2\equiv g_2(s). \tag{B3}$$

Model II.

$$g_l(s)=g_1(s), \tag{B4}$$

$$g_\nu(s)=s^{-3}(m_Y{}^2-s)(s-m_X{}^2)^2 \times[2s^2+s(m_Y{}^2+m_X{}^2)+2m_Y{}^2m_X{}^2]\equiv g_3(s), \tag{B5}$$

$$g_X(s)=(m_Y{}^2-m_X{}^2)^2+s(m_Y{}^2+m_X{}^2)-2s^2\equiv g_4(s). \tag{B6}$$

Model III.

$$g_l(s)=g_3(s), \tag{B7}$$

$$g_\nu(s)=g_1(s), \tag{B8}$$

$$g_X(s)=g_4(s). \tag{B9}$$

Note that this is the same as model II with l and ν interchanged.

The expressions for $dN/dp_\perp$ and dN/dE involve integrals of the g_i that can be evaluated explicitly: A list of these follows:

$$\int g_1(s)\,ds=-\tfrac{1}{3}s^3+\tfrac{1}{2}(m_Y{}^2+2m_X{}^2)s^2 - m_X{}^2(2m_Y{}^2+m_X{}^2)s+m_X{}^4m_Y{}^2\ln s, \tag{B10}$$

$$\int g_2(s)\,ds=\tfrac{1}{3}s^3-(m_Y{}^2+m_X{}^2)s^2+(m_Y{}^2-m_X{}^2)^2 s, \tag{B11}$$

$$\int g_3(s)\,ds=-\tfrac{2}{3}s^3+\tfrac{1}{2}(m_Y{}^2+3m_X{}^2)s^2 +m_Y{}^2(m_Y{}^2-3m_X{}^2)s+m_X{}^4(3m_Y{}^2-m_X{}^2)\ln s +m_Y{}^2m_X{}^4(3m_Y{}^2+m_X{}^2)s^{-1}-m_X{}^6m_Y{}^4s^{-2}, \tag{B12}$$

$$\int g_4(s)\,ds=-\tfrac{2}{3}s^3+\tfrac{1}{2}(m_Y{}^2+m_X{}^2)s^2+(m_Y{}^2-m_X{}^2)^2 s. \tag{B13}$$

These expressions simplify greatly in the limit of $m_X=0$ (see, e.g., the $dN/dp_{\perp l}$ formulas in Ref. 6), but this approximation is unjustified for the hadronic decays of interest.

APPENDIX C: CURRENT-FRAGMENTATION KINEMATICS

In order to carry out the multiple integral over x,y,z in Eq. (30), the following kinematic bounds must be obeyed.

Decay kinematics. For $E_e>\alpha m_Y=(m_Y{}^2-m_X{}^2)/$

$(2m_Y)$, there is a lower bound on $E_Y = zyE$ that leads to the following bound on z:

$$z \geq (E_e^2 + \alpha^2 m_Y^2)/(2\alpha y E E_e). \quad \text{(C1)}$$

In the kaon case, if $E_K \geq (m_Y^2 + m_K^2)/(2m_Y)$,

$$z \geq (\beta E_K - \gamma p_K)/(Ey), \quad \text{(C2)}$$

and for all E_K

$$z \leq (\beta E_K + \gamma p_K)/(Ey), \quad \text{(C3)}$$

where

$$\beta = (m_Y^2 + m_K^2)/(2m_K^2)$$

and

$$\gamma = (m_Y^2 - m_K^2)/(2m_K^2).$$

Y-production kinematics. The invariant mass squared of the final hadrons excluding the Y particle is

$$m_H^2 = [\nu(1-z) + M]^2 - [(\nu^2 + Q^2)^{1/2} - (\nu^2 z^2 - m_Y^2)^{1/2}]^2. \quad \text{(C4)}$$

The requirement $m_H^2 \geq M^2$ gives the following bound on z:

$$z \leq \frac{(\nu + M)(2M\nu - Q^2 + m_Y^2) + (\nu^2 + Q^2)^{1/2}[(2M\nu - Q^2 - m_Y^2)^2 - 4M^2 m_Y^2]^{1/2}}{2\nu(2M\nu + M^2 - Q^2)}. \quad \text{(C5)}$$

To order E^{-1} this bound reduces to

$$z \leq 1 - Mx^2/[2Ey(1-x)]. \quad \text{(C6)}$$

There is also a minimum z for Y produced at rest:

$$z \geq m_Y/(Ey). \quad \text{(C7)}$$

Current-fragmentation region. In order to avoid the target-fragmentation region, for which our Y-production model is not appropriate, we impose the restriction

$$z \geq z_0 \simeq 0.1\text{–}0.2. \quad \text{(C8)}$$

Threshold kinematics. The requirement that the hadronic invariant mass exceed $m_Y + M$ leads to

$$y(1-x) > (m_Y^2 + 2m_Y M)/(2ME). \quad \text{(C9)}$$

Deep-inelastic kinematics. The boundary of the deep-inelastic region to order E^{-1} is

$$0 \leq y \leq 1 - Mx/(2E), \quad 0 \leq x \leq 1. \quad \text{(C10)}$$

By integrating first over z, then y, then x, taking into account the various boundaries listed above, all integrations can be performed without recourse to Monte Carlo techniques, including a final spectrum average over E.

*Work supported in part by the University of Wisconsin Research Committee with funds granted by the Wisconsin Alumni Research Foundation, and in part by the Energy Research and Development Administration under Contract No. E(11-1)-881, COO-495.

[1]A. Benvenuti *et al.*, Phys. Rev. Lett. 34, 419 (1975); 35, 1199 (1975); 35, 1203 (1975); 35, 1249 (1975).

[2]B. C. Barish *et al.*, Phys. Rev. Lett. 36, 939 (1976); B. C. Barish *et al.*, Caltech Report No. 68-510, 1975 (unpublished); A. Bodek, Caltech Report No. 68-511, 1975 (unpublished).

[3]J. Von Krogh *et al.*, Phys. Rev. Lett. 36, 710 (1976).

[4]J. Blietschau *et al.*, Phys. Lett. 60B, 207 (1976).

[5]S. D. Drell and T.-M. Yan, Phys. Rev. Lett. 24, 855 (1970); P. V. Landshoff and J. C. Polkinghorne, Nucl. Phys. B33, 221 (1971); R. P. Feynman, *Photon-Hadron Interactions* (Benjamin, New York, 1972); M. Gronau *et al.*, Nucl. Phys. 51, 611 (1972); J. T. Dakin and G. J. Feldman, Phys. Rev. D 8, 2862 (1973); J. Cleymans and R. Rodenberg, *ibid.* 9, 155 (1974); C. H. Albright and J. Cleymans, Nucl. Phys B76, 48 (1974); L. M. Sehgal, *ibid.* B90, 471 (1975).

[6]L. M. Sehgal and P. Zerwas, Phys. Rev. Lett. 36, 399 (1976).

[7]C. Llewellyn Smith, Phys. Rep. 3C, 261 (1972).

[8]S. Glashow, J. Iliopoulos, and L. Maiani, Phys. Rev. D 2, 1285 (1970).

[9]R. Mohapatra, Phys. Rev. D 6, 2023 (1972); A. De Rújula *et al.*, Phys. Rev. Lett. 35, 69 (1975); Phys. Rev. D 12, 3589 (1975); S. Pakvasa *et al.*, Phys. Rev. Lett. 35, 702 (1975); F. Wilczek *et al.*, Phys. Rev. D 12, 2768 (1975); H. Fritzsch *et al.*, Phys. Lett. 59B, 256 (1975).

[10]C. Callan and D. Gross, Phys. Rev. Lett. 22, 156 (1969).

[11]E. G. Cazzoli *et al.*, Phys. Rev. Lett. 34, 1125 (1975).

[12]V. Barger *et al.*, SLAC Report No. SLAC-PUB-1688, 1975 (unpublished).

[13]R. Barnett, Harvard report, 1976 (unpublished); H. Georgi and D. Politzer, Harvard report, 1975 (unpublished).

[14]A. De Rújula *et al.*, Rev. Mod. Phys. 46, 391 (1974); S. Pakvasa *et al.*, Univ. Hawaii Report No. 511-207-75 (unpublished).

[15]J. Berge *et al.*, Report No. FERMILAB-PUB-75/84-EXP (unpublished).

[16]S. Barish *et al.*, Report No. ANL-HEP-CP-75-39 (unpublished).

[17]J. T. Dakin *et al.*, Phys. Rev. D 10, 1401 (1974).

[18]B. W. Lee, in *Proceedings of the 1975 International Symposium on Lepton and Photon Interactions at High*

Energies, Stanford, edited by W. T. Kirk (SLAC, Stanford University, Stanford, California, 1976), p. 635; J. Ellis *et al.*, Nucl. Phys. B100, 313 (1975).
[19] B. Knapp *et al.*, Phys. Rev. Lett. 34, 1044 (1975); G. Blanar *et al.*, *ibid.* 35, 346 (1975); F. Halzen and W. F. Long, Univ. of Wisconsin at Madison Report No. COO-480, 1975 (unpublished).
[20] J. LoSecco, Phys. Rev. Lett. 36, 336 (1976).
[21] M. L. Perl *et al.*, Phys. Rev. Lett. 35, 1489 (1975).
[22] I. Karliner, Phys. Rev. Lett. 36, 759 (1976).